

Article

Structure of Cubic Al_{73.8}Pd_{13.6}Fe_{12.6} Phase with High Al Content

Hao Li and Changzeng Fan *

State Key Laboratory of Metastable Materials Science and Technology, Yanshan University, Qinhuangdao 066004, China; lihao@stumail.ysu.edu.cn

* Correspondence: chzfan@ysu.edu.cn; Tel.: +86-335-805-7047

Received: 4 September 2019; Accepted: 10 October 2019; Published: 13 October 2019



Abstract: A cubic ternary phase Al_{73.8}Pd_{13.6}Fe_{12.6} (designated C' phase), with very high Al content (Al/TM = 2.82, TM denotes transition metal) was prepared by spark plasma sintering (SPS). Its crystal structure was determined by combining single-crystal X-ray diffraction (SXR) and scanning electron microscope (SEM) equipped with energy dispersive X-ray spectroscopy (EDS) measurements. The crystal structure of the new phase can be described with a small unit cell ($a = 7.6403(2)$ Å; space group $Pm\bar{3}$, No. 200) as that of Al_{2.63}Rh ($a = 7.6692(1)$ Å; space group $P23$, No. 195) while different from those of the reported Al₃₉Pd₂₁Fe₂ ($a = 15.515(1)$ Å; space group $Fm\bar{3}$, No. 202) and Al₆₉Pd₁₇Fe₁₄ ($a = 15.3982(2)$ Å; space group $Im\bar{3}$, No. 204) compounds, which both adopt a double length unit cell in the Al–Pd–Fe system. The mechanism of distributing more Al atoms in the new phase was compared with that of the Al_{2.63}Rh phase by analyzing their site symmetry and the corresponding site of occupancies (SOF). Furthermore, relations of the C' phase to the reported Al₆₉Pd₁₇Fe₁₄ (designated C1 phase) and Al₃₉Pd₂₁Fe₂ (designated C2 phase) phases were investigated by analyzing their building units with the “nanocluster” method in the ToposPro package.

Keywords: quasicrystals; intermetallic; crystal structure; disorder; topological analysis

1. Introduction

Since the discovery of quasicrystals (QCs) by Shechtman et al., many stable three-dimensional (3D) icosahedral, two-dimensional (2D) decagonal, as well as one-dimensional (1D) quasicrystals have been found in the Al–Cu–TM and Al–Pd–TM systems (where “TM” indicates a transition metal) [1–5]. The Al–Cu–Fe and Al–Pd–Mn QCs have been extensively studied due to their stability, unique structural model, and potential industrial applications, such as wear-resistant coatings [6–10]. The formation, phase stability, and structure of Al–Cu–Fe QCs have been notably studied since the first natural QCs discovered in the Al–Cu–Fe system a decade ago [11–21]. Meanwhile, a variety of Al-based complex metallic phases have been synthesized and analyzed as their chemical compositions and crystal structures are quite similar to their quasicrystal counterparts [22–26].

Both the quasicrystals and their approximants in the Al–Pd–Fe alloys have been the subject of extensive research for their similarity and diversity of phases with those in the Al–Cu–Fe and Al–Pd–Mn alloys [8,27–29]. During the past thirty years, several stable 2D and 1D quasicrystals and metastable 3D quasicrystals, as well as some quasicrystal approximants in the Al–Pd–Fe alloy, have been reported [5,30–35]. For clarity, most known phases with their stoichiometry range in the ternary diagram of Al–Pd–Fe described by Balanetsky et al. are reproduced and shown in Figure 1 [34]. A stable cubic approximant phase with nominal composition, Al₇₀Pd₁₀Fe₂₀ was found to coexist with a decagonal phase and an icosahedral phase in the melt-quenched Al–Pd–Fe alloys [5]. A few years later, it was confirmed that the metastable icosahedral phase was first formed by rapid quenching (obtained by melt spinning with a 20 cm diameter copper roller rotating at 6000 rpm) in the liquid

with nominal composition $\text{Al}_{70}\text{Pd}_{10}\text{Fe}_{20}$ and then transformed to the cubic phase with a period of about 20.5 Å (obtained by slow cooling and full annealing) [30]. In another work, the crystal structure of $\text{Al}_{39}\text{Pd}_{21}\text{Fe}_2$ (the C2 phase) has been solved and refined with a large unit cell (space group $Fm\bar{3}$; $a = 15.515$ Å.) [32]. An untrivial ordering scheme was observed by analyzing its relationships with other Al–TM compounds, and consequently a plausible geometrical model was derived for static disorder concerning certain Al sites. The structures of two other cubic approximants $\text{Al}_{63.6}\text{Pd}_{30.2}\text{Fe}_{6.2}$ and $\text{Al}_{68.9}\text{Pd}_{17.1}\text{Fe}_{13.9}$ with space groups $Fm\bar{3}$ and $Im\bar{3}$, respectively, have been found by single-crystal X-ray diffraction measurements [22]. However, the structure of $\text{Al}_{68.9}\text{Pd}_{17.1}\text{Fe}_{13.9}$ (designated C1 phase, with a concise formula $\text{Al}_{69}\text{Pd}_{17}\text{Fe}_{14}$) was updated with space group $Im\bar{3}$ in another work [31]. Note that the Al concentration in the $\text{Al}_{63.6}\text{Pd}_{30.2}\text{Fe}_{6.2}$ and $\text{Al}_{68.9}\text{Pd}_{17.1}\text{Fe}_{13.9}$ phase is quite close to that of the $\text{Al}_{39}\text{Pd}_{21}\text{Fe}_2$ and $\text{Al}_{70}\text{Pd}_{10}\text{Fe}_{20}$ phase, respectively.

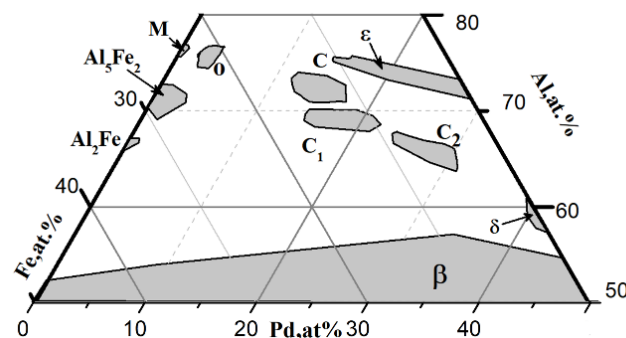


Figure 1. Overall compositions of the high-Al Al–Pd–Fe phases between 1020 °C and 900 °C; Region of the ϵ -phases is given for 750 °C. (M: monoclinic M- $\text{Al}_{13}\text{Fe}_4$; O: orthorhombic O- $\text{Al}_{13}(\text{Fe},\text{Pd})_4$; δ : Al_3Pd_2 ; β : $\text{Al}(\text{Pd},\text{Fe})$; ϵ : Al_3PdF_x (the x component is between 0% and 10%); C-phase: in a compositional range of 1–2 at.% around $\text{Al}_{71.5}\text{Pd}_{15.0}\text{Fe}_{13.5}$; C₁-phase: in a compositional range between $\text{Al}_{69.5}\text{Pd}_{14.8}\text{Fe}_{15.7}$ and $\text{Al}_{68.5}\text{Pd}_{22.2}\text{Fe}_{9.3}$; C₂-phase: in a compositional range around $\text{Al}_{67.0}\text{Pd}_{24.5}\text{Fe}_{8.5}$).

These approximants to the icosahedral phase in the Al–Pd–Fe system have been summarized as the C phase with formula $\text{Al}_{72.8}\text{Pd}_{14.3}\text{Fe}_{12.9}$ ($Pm\bar{3}$, $a = 7.655$ Å), the C1 phase with formula $\text{Al}_{68.2}\text{Pd}_{21.4}\text{Fe}_{10.4}$ ($Im\bar{3}$, $a = 15.389$ Å), and the C2 phase with formula $\text{Al}_{64.3}\text{Pd}_{30.3}\text{Fe}_{5.4}$ ($Fm\bar{3}$, $a = 15.515$ Å) in comprehensive work by Balanetsky et al. In this work, scanning and transmission electron microscopy with electron-probe microanalysis was combined with X-ray structure analysis and used to study their mutual transformations and orientation relationships [33]. Despite the aforementioned extensive efforts, the crystal structure of the C phase has not been determined.

In the present work, we report the detailed crystal structure analysis of a cubic ternary $\text{Al}_{73.9}\text{Fe}_{13.7}\text{Pd}_{12.4}$ phase (designated C' phase as its composition is slightly different than that of the C phase) with very high Al content. The sample was prepared using the spark plasma sintering (SPS) approach when revisiting the $\text{Al}_{75}\text{Pd}_{15}\text{Fe}_{10}$ 2D quasicrystals and its cubic approximants [34,35]. Furthermore, its similarity and difference with the reported C1, C2 phases and $\text{Al}_{2.63}\text{Rh}$ are discussed.

2. Materials and Methods

Pure elements (Al 99.8%, Pd 99.95%, Fe 99.8%) were mixed in the stoichiometric ratio 75:15:10, ground and homogenized in an agate mortar. The blended powders were then packed with graphite paper and filled into a graphite die, which was placed between the upper and lower conductive plates of the SPS machine. The graphite die was then set to the pressure value of ~50 MPa, with a sintering temperature of 1100 °C and a high vacuum of 6×10^{-3} Pa in Ar atmosphere. These conditions were maintained for 10 minutes and then cooled rapidly to room temperature by shutting off the power. Finally, the sintered block was removed from the graphite die and broken into small pieces.

The SPS specimens were cut to a size 12 mm \times 10 mm \times 4 mm, then wrapped in phenolic powders and heated to 140 °C for 10 minutes. After cooling in water, the specimens were ground with 400 to

2000 grit silicon carbide paper and polished with W2.5 artificial diamond paste. Next, the specimens were treated by surface erosion with a self-prepared erosion agent (HF: 2 mL; HCl: 3 mL; HNO₃: 5 mL; and H₂O: 190 mL), followed by cleaning and drying with distilled water and ethanol. A scanning electron microscope (SEM, Hitachi S-3400N type, Hitachi, Tokyo, Japan) equipped with EDS (EDAX Inc., Mahwah, NJ, USA) at a cathode voltage of 20 kV and a current of 80 mA was used to characterize the morphology and chemical composition. The chemical compositions of each element were analyzed by comparing the integrated net intensities with corresponding data collected automatically by the EDAX Inc. Two standard samples (pure aluminum and copper) were adopted to calibrate the peak positions from time to time. A fragment of single crystal with dimensions 105 × 75 × 40 μm³ was selected by a polarizing microscope (LEICA DM4 M) for diffraction measurements with a four-circle single-crystal X-ray diffractometer (Bruker D8 venture, Bruker AXS GmbH, Karlsruhe, Germany). All data processing was performed with the APEX3 program suit, including data reduction by SAINT, absorption correction by SADABS, structural solving and refinement by SHELXT and SHELXL [36–38], respectively. The topological features of the discovered C' phase with the available C1 and C2 phases were analyzed by the nanocluster approach implanted in the ToposPro package [39–42].

3. Results and Discussion

3.1. Microstructure

The microstructure of the SPS sample after polishing and etching is shown by the SEM images in Figure 2a–c. From Figure 2a one can observe that some parts of the surface were scratched off during polishing and plenty of gear-shaped single-crystal pillars showed up at these sites. There were four common regions (denoted as A, B, C, E) and one special region where the gear-shaped single crystal was located (denoted as D), as illustrated by the different contrast images in Figure 2b,c, which was further confirmed by the EDS analysis results listed in Table 1. Figure 2d shows the morphology of the selected specimen fragment after the single-crystal XRD measurements, and the chemical composition in region F was used as a reference during the following structural refinement of the discovered C' phase. The recovered phases should not be chemical equilibrium phases and the possible phases for each region are shown in Table 1. Concerning the chemical composition uncertainties for each phase (especially for the element iron), with some regions like region C and D it is difficult to distinguish between the ε phase and QCs phase.

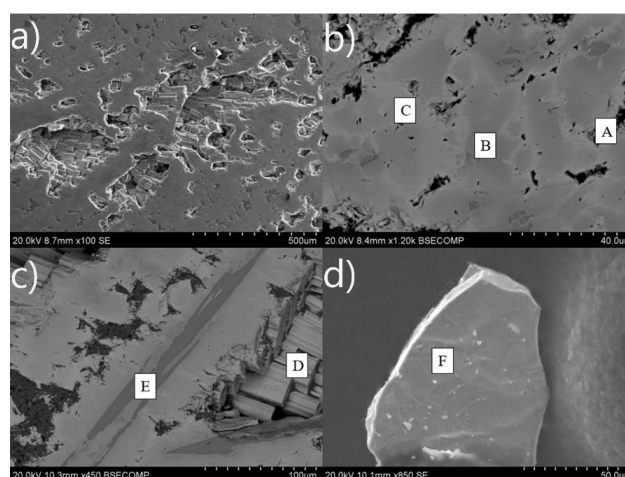


Figure 2. Scanning electron microscope (SEM) micrographs and energy dispersive X-ray spectroscopy (EDS) analysis of Al–Pd–Fe samples prepared by SPS. (a–c) reveal the as-cast state and (d) the fragment of measured single crystal. (a) and (d) were taken with secondary electron (SE), (b) and (c) were taken with back-scattered electron (BSE). EDS analysis was performed on different sites of the denoted regions A–F and results are listed in Table 1.

Table 1. The chemical compositions of a piece of educts and a fragment of single crystal from the spark plasma sintering samples analyzed by the EDS (bold numbers indicate the mean values of different measured chemical compositions in the same region). Regions A–F are denoted in Figure 2.

Region	Image Contrast	x(Al)/%	x(Pd)/%	x(Fe)/%	Possible Phase
A	Dark	100 (\pm 1.13)	0	0	Pure Al
B	Dark grey	76.29 (\pm 5.45)	14.48 (\pm 2.48)	9.22 (\pm 4.02)	C- or C'-phase ¹
		76.31 (\pm 5.45)	14.76 (\pm 2.66)	8.93 (\pm 4.17)	
		77.09 (\pm 5.36)	12.97 (\pm 2.55)	9.94 (\pm 3.73)	
		76.56 (\pm 5.43)	14.39 (\pm 2.60)	9.05 (\pm 4.13)	
		76.66 (\pm 5.42)	14.41 (\pm 2.46)	8.94 (\pm 4.04)	
		76.6 (\pm 5.4)	13.0 (\pm 2.6)	9.2 (\pm 4.0)	
C	Bright	75.60 (\pm 5.52)	21.26 (\pm 2.28)	3.14 (\pm 10.49)	ϵ -phase ² or QCs ³
		76.02 (\pm 5.48)	19.87 (\pm 2.32)	4.11 (\pm 7.53)	
		75.8 (\pm 5.5)	20.6 (\pm 2.3)	3.6 (\pm 9.0)	
D	gear-shaped	77.01 (\pm 5.40)	19.26 (\pm 2.34)	3.74 (\pm 8.68)	QCs ³ or ϵ -phase ²
		78.43 (\pm 5.29)	18.33 (\pm 2.45)	3.24 (\pm 9.03)	
		76.19 (\pm 5.48)	21.07 (\pm 2.31)	2.75 (\pm 11.30)	
		77.2 (\pm 5.4)	19.6 (\pm 2.4)	3.2 (\pm 9.7)	
E	Gray stripe	77.22 (\pm 5.31)	3.90 (\pm 4.62)	18.88 (\pm 2.59)	Fe-rich phase ⁴
		77.13 (\pm 5.32)	3.81 (\pm 4.68)	19.05 (\pm 2.58)	
		76.89 (\pm 5.43)	4.01 (\pm 4.01)	19.10 (\pm 2.59)	
		77.1 (\pm 5.4)	3.9 (\pm 4.4)	19.0 (\pm 2.6)	
F	Single crystal	74.28 (\pm 5.69)	12.38 (\pm 3.03)	13.34 (\pm 3.89)	C'-phase
		74.00 (\pm 5.72)	11.84 (\pm 3.12)	14.17 (\pm 3.67)	
		73.85 (\pm 5.76)	12.07 (\pm 3.30)	14.08 (\pm 3.71)	
		74.0 (\pm 5.7)	12.1 (\pm 3.2)	13.9 (\pm 3.8)	

¹ C'-phase is slightly different from the C-phase mentioned in [43]. ² Chemical composition range fits that of the ϵ -phase [34,44]. ³ Chemical composition range disagrees with that of reported decagonal quasicrystal. However, ten-fold X-ray diffraction patterns were observed and will be discussed elsewhere (see Figure S1 in the Supplementary Materials). ⁴ The Fe-rich phase has been described as O-Al₃Fe in [45], as well as O-Al₁₃(Pd, Fe)₄ in [34].

The chemical composition of the gear-shaped single-crystal (Region D) was found to scatter with the concentration of the quasicrystal phase, although ten-fold X-ray diffraction patterns suggested the formation of quasicrystals (see Figures S1 and S2 in the Supplementary Materials to compare the projected diffraction patterns of the quasicrystals and the cubic C' phase discussed here). However, this is beyond the scope of the present study. Concerning the selected fragment of the single-crystal sample, EDS analysis was carried out on three areas (Region F) which provided an average chemical composition of Al_{74.0}Pd_{12.1}Fe_{13.9}. This fits well with the refined model with the measured single-crystal X-ray diffraction data sets.

3.2. Crystal Structure Determination

The structure model was solved with space group $Pm\bar{3}$ (No. 200) by direct method. The crystal data, data collection, and structure refinement details are summarized in Table 2. The crystal was refined with PART and EADP commands for TM2 atoms (Pd/Fe co-occupied position, see Table 3). The site occupancy factor (SOF) of Pd2 was refined to be 0.473(84). The detailed crystal structure information of the present phase was accepted by the Cambridge Crystallographic Data Centre (CCDC) with deposition number 1897801. All data sets collected by a four-circle single-crystal X-ray diffractometer (Bruker D8 Venture, Bruker AXS GmbH, Karlsruhe, Germany) have been published at the public repository Mendeley Data: <https://data.mendeley.com/datasets/538y46cpmh/1>.

Note that the $P23$ space group was also applied to solve and refine the new phase (see Table S1 of the Supplementary Materials). However, it was not adopted, as the refinement indicators (e.g., R_1 , ωR_2 and $\Delta\rho_{\max}$, $\Delta\rho_{\min}$) became much worse. The disorder discussed in the present work mainly concerns the vacancies/co-occupied positions and positional disorder as reflected by site occupancy factors and unreasonable short length bonds. Stream-like diffuse scattering features (see Figure S2d–f of the

Supplementary Materials) are ignored when processing the single-crystal X-ray diffraction datasets by the APEX3 suit program.

Table 2. The crystallographic data of the C'-phase.

Chemical Formula		Crystal Data	
		Al _{5.64} Pd _{1.04} Fe _{0.96} (Al _{73.8} Pd _{13.6} Fe _{12.6})	
Crystal system		Cubic	
Space group		$Pm\bar{3}$	
$a, b, c/\text{\AA}$		7.6403(2)	
$\alpha, \beta, \gamma/^\circ$		90	
$V/\text{\AA}^3$		446.00(4)	
Z		4	
Intensity Measurements			
Radiation		Mo-K α , $\lambda = 0.71073$ (Å)	
μ/mm^{-1}		8.231	
Diffractometer		Bruker D8 Venture Photon 100 CMOS	
Radiation absorption correction		Multi-scan	
T_{\min}, T_{\max}		0.757, 0.870	
No. measured reflections		15,873	
No. unique reflections		230	
No. observed reflections ($I > 2\sigma(I)$)		223	
R_{int}		0.0372	
$(\sin \theta/\lambda)_{\max}$ (Å ⁻¹)		0.987	
Refinement of the Structure			
No. parameters used in refinement		34	
No. reflections used in refinement		223	
R_1 ($F_{\text{obs}} > 4\sigma(F_{\text{obs}})$)		0.0286	
R_1 (all data)		0.0300	
ωR_2 ($F_{\text{obs}} > 4\sigma(F_{\text{obs}})$)		0.0860	
ωR_2 (all data)		0.0888	
$\Delta\rho_{\max}, \Delta\rho_{\min}$ (e Å ⁻³)		0.847, -0.992	

Table 3. The atomic positions of the C'-phase (in gray) compared to those of the Al_{2.63}Rh phase (Occ. indicates the site occupancy factor).

Label	Site	x	y	z	Occ.	U _{eq} , U _{iso}
Pd1	1b	$\frac{1}{2}$	$\frac{1}{2}$	$\frac{1}{2}$	1.0000	0.0056(5)
Rh1	1b	$\frac{1}{2}$	$\frac{1}{2}$	$\frac{1}{2}$	1.0000	0.007
TM2	6f	$\frac{1}{2}$	0.70685(12)	0	0.526(13) Pd 0.474(13) Fe	0.0116(4)
Rh3	6h	$\frac{1}{2}$	0	0.2931(4)	1.0000	0.013
Fe1	1a	0	0	0	1.0000	0.0054(7)
Rh2	1a	0	0	0	1.0000	0.011
Al1	12k	$\frac{1}{2}$	0.8048(3)	0.6817(3)	1.0000	0.0111(6)
Al1	12j	0.2004	0.5004	0.6773	1.0000	0.013
Al2	8i	0.8154(4)	0.8154(4)	0.8154(4)	0.629(14)	0.0288(17)
Al2	4e	0.8243	0.8243	0.8243	1.0000	0.017
Al3	6e	0.387(3)	0	0	0.40(2)	0.072(7)
Al3	6f	0	0	0.3910	0.2600	0.025
Al4	12j	0.705(2)	0	0.878(2)	0.163(13)	0.029(6)
Al4	12j	0.1230	0.0160	0.3010	0.1400	0.032
Al5	12j	0.723(4)	0.864(4)	0	0.102(13)	0.036(10)
Al5	12j	0.1810	0.1330	0.2280	0.1500	0.025

For the convenience of the following discussion, bond lengths for the C'-phase are listed in Table S2 of the Supplementary Materials. The coordination polyhedra formed around Fe1 and Pd1 atoms are illustrated in Figure S3 of the Supplementary Materials where the distances to the vertices are also

listed. The detailed crystallographic information of C1, C2, and C phases are attached in Table S3 of the Supplementary Materials in the study of the group–subgroup relationship through the construction of the Bärnighausen tree approach for interested readers [46,47].

There are five Al and three TM determined sites in the refined structural model, as shown in Table 3 and Figure 3a. One TM site is occupied by a mixture of Fe and Pd atoms and the remaining two are fully occupied by Fe and Pd, respectively. Only one Al (Al1) site is fully occupied and the rest are partially occupied. Among these partially occupied Al sites, the SOF of Al2 is 0.629(14) but those of Al3, Al4, and Al5 sites are all lower than 0.5. The last three sites are quite close to each other and have quite abnormal anisotropic parameters. The atomic displacement parameters (ADPs) of these partially occupied Al sites are all very large, especially those of Al3 site atoms refined to be 0.072(7), implying disorder should exist at these positions. Note that the ADPs of the Al5 site have to be isotropic, otherwise the crystal structure would collapse. Considering the short distance between these three sites ($\text{Al3–Al4} = 1.40(3) \text{ \AA}$, $\text{Al3–Al5} = 1.34(4) \text{ \AA}$, $\text{Al4–Al5} = 1.17(3) \text{ \AA}$), one can deduce that all of these should be divided from the same atomic position.

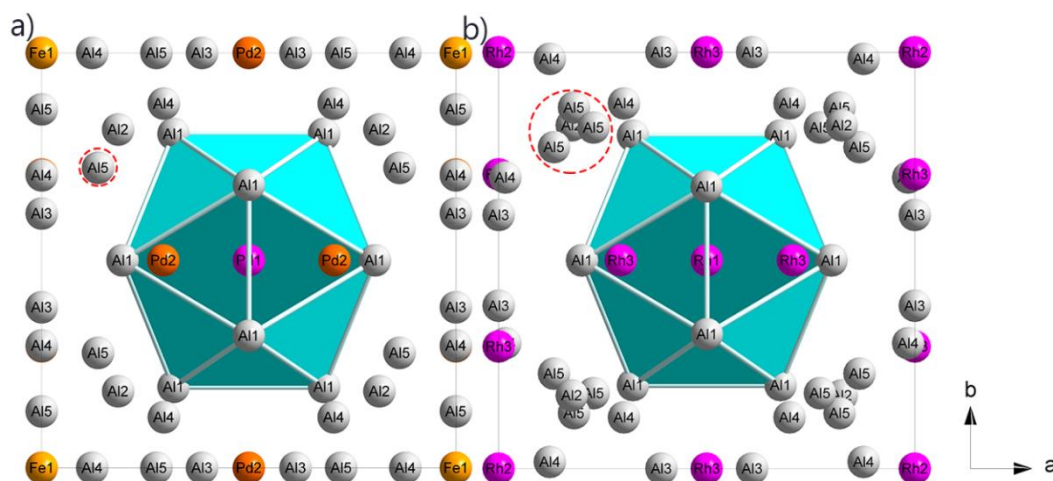


Figure 3. The crystal structure of the C' -phase (a) and the $\text{Al}_{2.63}\text{Rh}$ phase (b) projected along the [001] direction. (Graphs prepared by DIAMOND [48]).

It was found that the C' -phase was still an isotype of the typical $\text{Al}_{2.63}\text{Rh}$ phase, as shown in Figure 3b, and both had an identical framework, mainly composed of TM atoms [49]. The crystal structure of the $\text{Al}_{2.63}\text{Rh}$ phase was refined in the non-centrosymmetric $P23$ space group and also adopted small unit cells as the C' -phase. There were five fully occupied (Rh1, Rh2, Rh3, Al1, and Al2) atoms and three partially occupied (Al3, Al4, and Al5) atoms in the $\text{Al}_{2.63}\text{Rh}$ structure (refer to Table 3). From Table 3, it can be seen that Pd1 (Rh1), Fe1 (Rh2), and TM2 (Rh3) occupied the same Wyckoff position, which were located at the center, corner and face of the unit cell of the C' -phase ($\text{Al}_{2.63}\text{Rh}$), respectively.

Contrary to the nearly identical TM atoms, there were some differences between the light atoms, except for the Al1 atoms of the C' -phase and the $\text{Al}_{2.63}\text{Rh}$ phase which resulted in a higher concentration of Al in the former phase. Firstly, different site symmetry of Al2 atoms contributed to more light atoms in the C' -phase, although its SOF was much lower than that of the $\text{Al}_{2.63}\text{Rh}$ phase. Secondly, Al3 and Al4 atoms had the same site symmetry in both phases but had larger SOF in the C' -phase than that of the $\text{Al}_{2.63}\text{Rh}$ phase, which contributed to more light atoms. Finally, the Al5 atoms contributed to slightly fewer light atoms in the C' -phase than that of the $\text{Al}_{2.63}\text{Rh}$ phase. To summarize, there were more Al atoms in the unit cell of the C' -phase which resulted in a higher Al content ($\text{Al/TM} = 2.82$) than that of the $\text{Al}_{2.63}\text{Rh}$ phase. This Al/TM ratio value of 2.82 is the highest among the Al–Pd–Fe system, although it is still not comparable to those in the Al–Cu–Fe system (e.g., an Al/TM ratio value of 3.17 in a recently discovered $\lambda\text{-Al}_{13}\text{Fe}_4$ -type intermetallic $(\text{Al,Cu})_{13}(\text{Fe,Cu})_4$ compound [50]).

3.3. Topological Features

Relations of the C' -phase to the reported C1 ($\text{Al}_{69}\text{Pd}_{17}\text{Fe}_{14}$) and C2 ($\text{Al}_{39}\text{Pd}_{21}\text{Fe}_2$) phases were investigated by analyzing their building units with the “nanocluster” method integrated in the ToposPro package [39]. It was found that the arrangement of atomic clusters in all aforementioned three phases could simply be described as an icosahedra cluster centered at a Pd atom plus eight identical (C') or different (C1 and C2) polyhedron clusters, as illustrated in Figures 4 and 5.

For the C' -phase, the first building unit is an icosahedra cluster composed of a centered Pd (Pd1) atom located at Wyckoff position 1b ($\frac{1}{2}, \frac{1}{2}, \frac{1}{2}$) and 12 Al (Al1) atoms occupying the 12k Wyckoff position forming an icosahedron as shown in Figure 4a. The atomic distance between Al1 and Pd1 atoms equals 2.711 Å. The second building unit is a complex double-shell cluster centered at the Fe (Fe1) atom. The first shell (inner-shell) is composed of 32-coordinated atoms (Al2, Al4, and Al5), forming an irregular polyhedron as shown in Figure 4b. The atomic distance between the centering Fe1 and Al2, Al4, and Al5 equals 2.433 Å, 2.358 Å, and 2.437 Å, respectively. The second shell (outer-shell) is composed of 48-coordinated atoms including 12 Al3 atoms, 24 Al1 atoms, and 12 Pd2 atoms as shown in Figure 4c. Note that all the Al1 atoms are shared with the surrounding first building units as shown in Figure 4d. The two building units are closely connected to form the global crystal structure of the C' -phase as shown in Figure 4e.

For the C1 ($\text{Al}_{69}\text{Pd}_{17}\text{Fe}_{14}$) and C2 ($\text{Al}_{39}\text{Pd}_{21}\text{Fe}_2$) phases, both are described by the supercell of the basic $\text{Al}_{2.63}\text{Rh}$ phase and have lower Al element content and a higher degree of disorder than the present C' -phase. It was also found that both of the C1 and C2 phases have three building units by the “nanocluster” method [39]. Both of them had an icosahedron cluster centered at the Pd atom (1st building unit, Figure 5a,a*) and a complicated double-shell cluster centered Al/Fe atom (second building unit, Figure 5e). The double-shell cluster is composed of a 14-coordinated (8 Pd atoms and 6 Al atoms) first shell (inner-shell) and a 48-coordinated (36 Al atoms plus 12 Pd atoms) second shell (outer-shell) as shown in Figure 5d,e. The third building unit of the C1 and C2 phases is an 18-coordinated spindle-shaped cluster centered at the Fe atom (Figure 5c), and a 20-coordinated dodecahedron cluster centered at the Fe/Pd atom (Figure 5b), respectively. There are six spindle-shaped clusters plus two double-shell clusters in the C1 phase, while there are four dodecahedron clusters plus four double-shell clusters in the C2 phase surrounding their centered icosahedron cluster. It can be deduced that the different Al content (Al/TM) in the C1 and C2 phases is mainly caused by the eight different clusters surrounding the icosahedron cluster, although both have similar topological features.

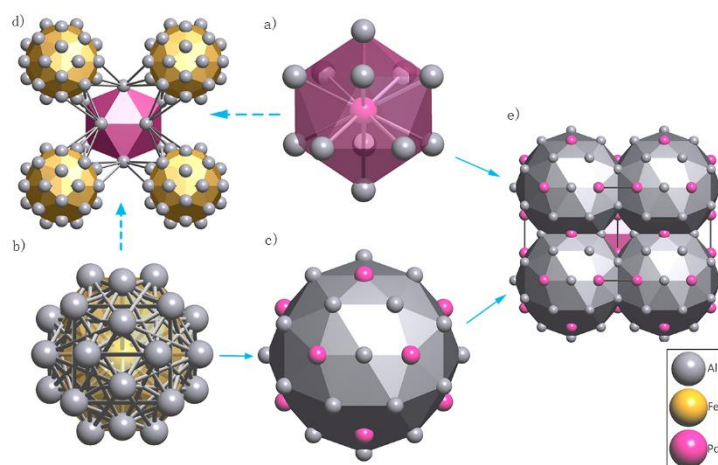


Figure 4. Building units and their packing around high symmetric positions in the C' -phase. (a): the first building unit which is an icosahedra cluster; (b) the inner-shell of the second building unit; (c) the outer-shell of the second building unit; (d) packing pattern of one first building unit and four inner-shells; (e) packing pattern of one first building unit and four second building units.

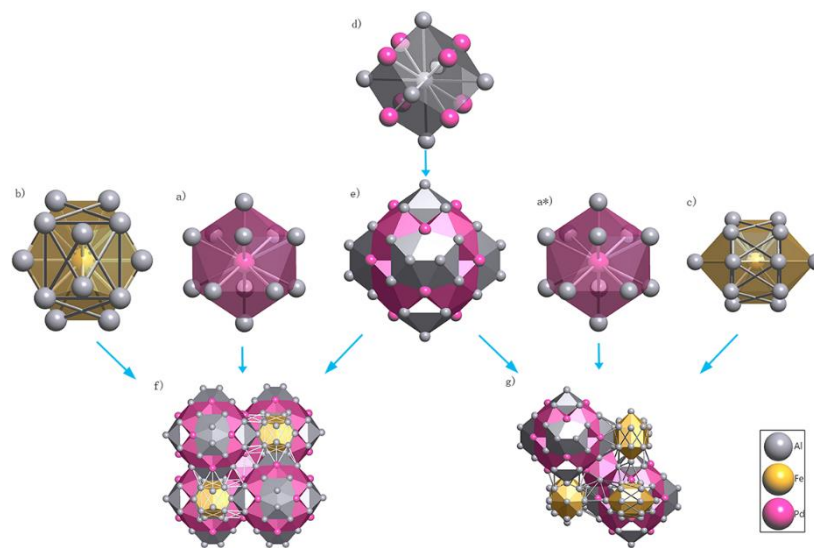


Figure 5. Building units and their packing around high symmetric positions in the C1 and C2 phases. (a) and (a*): the first building unit which is an icosahedra cluster; (b) the third building unit of the C2 phase; (c) the third building unit of the C1 phase; (d) the inner-shell of the second building unit; (e) the outer-shell of the second building unit; (f) packing pattern of the C2 phase; (g) packing pattern of the C1 phase.

One can easily conclude that all three of the aforementioned phases can be simply described as an icosahedron cluster centered at a Pd atom plus eight identical (C') or different (C1 and C2) polyhedron clusters. In other words, the C' , C1, and C2 phases are mainly distinguished from their second and third building units. The C1 and C2 phases have a different second building unit and additional third building unit from those of the C' phase. There are 2(4) second building and 6(4) third building units to total eight clusters surrounding the first building unit for the C1 (C2) phase. It is the different type and number of second and third building units, as well as the site of occupancy, that decides the different content of Al elements in these three phases.

4. Conclusions

In summary, the crystal structure of a cubic ternary phase $\text{Al}_{73.8}\text{Pd}_{13.6}\text{Fe}_{12.6}$ (designated C' phase) synthesized by SPS approach with very high Al content ($\text{Al}/\text{TM} = 2.82$) was solved and refined by combing SXR and SEM/EDS measurements. The crystal structure of the C' phase can be described by a small unit cell ($a = 7.6403(2) \text{ \AA}$) with space group $Pm\bar{3}$ (No. 200). It is deduced that a higher Al content in the C' -phase than that of the $\text{Al}_{2.63}\text{Rh}$ phase can be mainly attributed to the different site symmetry and SOF of Al atoms located at the $8i$ Wyckoff position. Furthermore, it was found that the C' phase, the C1 ($\text{Al}_{69}\text{Pd}_{17}\text{Fe}_{14}$), and C2 ($\text{Al}_{39}\text{Pd}_{21}\text{Fe}_2$) phases have an identical icosahedron building unit centered at a Pd atom with different configurations of surrounding eight building units, resulting in different aluminum element content in these three phases. As an important quasicrystal approximant phase, the discovery and study of the C' phase would stimulate more experimental or theoretical efforts focusing on the intermetallic compounds and phase diagram of the Al–Pd–Fe ternary system.

Supplementary Materials: The following are available online at <http://www.mdpi.com/2073-4352/9/10/526/s1>, Figure S1: Projected diffraction patterns along the periodic direction of the quasicrystal phase, Figure S2: Projected diffraction patterns along a: $\langle 100 \rangle$, b: $\langle 010 \rangle$ and c: $\langle 001 \rangle$ directions and the corresponding unwarp images along e: $\langle 100 \rangle$, f: $\langle 010 \rangle$ and g: $\langle 001 \rangle$ directions for the C' -phase of Al–Pd–Fe, Figure S3: Environments of a: Pd1 and b: Fe1 atoms for the C' -phase, Table S1: The crystallographic data of the C' -phase in space group $Pm\bar{3}$, Table S2: Geometric parameters: Bond lengths (\AA) for C' -phase in space group $Pm\bar{3}$, Table S3: Crystallographic information of C1, C2 and C phases.

Author Contributions: Conceptualization, C.F.; investigation, H.L. and C.F.; writing—original draft preparation, H.L.; writing—review and editing, C.F.; project administration, C.F.; funding acquisition, C.F.

Funding: This research was funded by Research Foundation of Education Bureau of Hebei Province (grant number ZD2018069) and The APC was funded by the Hebei Province Youth Top-notch Talent Program (2013–2018).

Acknowledgments: This work benefited from the insightful comments and suggestions of two anonymous referees.

Conflicts of Interest: The authors declare no conflict of interest.

References

1. Shechtman, D.; Blech, I.; Gratias, D.; Cahn, J.W. Metallic phase with long-range orientational order and no translational symmetry. *Phys. Rev. Lett.* **1984**, *53*, 1951–1953. [[CrossRef](#)]
2. Steurer, W. Quasicrystals: What do we know? What do we want to know? What can we know? *Acta Crystallogr. A* **2018**, *74*, 1–11. [[CrossRef](#)] [[PubMed](#)]
3. Senabulya, N.; Xiao, X.; Han, I.; Shahani, A.J. On the kinetic and equilibrium shapes of icosahedral Al₇₁Pd₁₉Mn₁₀ quasicrystals. *Script. Mater.* **2018**, *146*, 218–221. [[CrossRef](#)]
4. Strzalka, R.; Buganski, I.; Kuczera, P.; Pytlik, L.; Wolny, J. Atomic structure of decagonal Al-Cu-Rh quasicrystal-revisited. *Crystals* **2019**, *9*, 78. [[CrossRef](#)]
5. Tsai, A.P.; Yamamoto, A. Stable one-dimensional quasicrystals in Al-Pd-Fe alloys. *Philos. Mag. Lett.* **1992**, *66*, 203–208. [[CrossRef](#)]
6. Tsai, A.P.; Inoue, A.; Masumoto, T. A Stable Quasicrystal in Al-Cu-Fe System. *Jpn. J. Appl. Phys.* **1987**, *26*, L1505–L1507. [[CrossRef](#)]
7. Quiquandon, M.; Gratias, D. Unique six-dimensional structural model for Al-Pd-Mn and Al-Cu-Fe. *Phys. Rev. B* **2006**, *74*, 214205. [[CrossRef](#)]
8. Beauchesne, J.T.; Caillard, D.; Momprou, F.; Ochin, P.; Quiquandon, M.; Gratias, D. Study of quasicrystals obtained from a structural model of icosahedral phases of type F AlPdMn/AlCuFe. *Z. Kristallogr.* **2008**, *223*, 823–826. [[CrossRef](#)]
9. Divincenzo, D.P.; Krakow, W.; Bancel, P.A. An atomic model of Al-Cu-Fe, and its comparison with high-resolution electron microscope images. *J. Non-Crystal. Solids* **1993**, *153–154*, 145–149. [[CrossRef](#)]
10. Chen, Y.J.; Qiang, J.B.; Dong, C. Smearing-type wear behavior of Al₆₂Cu_{25.5}Fe_{12.5}. *Intermetallics* **2016**, *68*, 23–30. [[CrossRef](#)]
11. Bindi, L.; Eiler, J.M.; Guan, Y.B.; Hollister, L.S.; MacPherson, G.; Steinhardt, P.J.; Yao, N. Evidence for the extraterrestrial origin of a natural quasicrystal. *Proc. Natl. Acad. Sci. USA* **2012**, *109*, 1396–1401. [[CrossRef](#)] [[PubMed](#)]
12. Hollister, L.S.; Bindi, L.; Yao, N.; Poirier, G.R.; Andronicos, C.L.; MacPherson, G.J.; Lin, C.; Distler, V.V.; Eddy, M.P.; Kostin, A.; et al. Impact-induced shock and the formation of natural quasicrystals in the early solar system. *Nat. Comm.* **2014**, *5*, 4040. [[CrossRef](#)] [[PubMed](#)]
13. Asimow, P.D.; Lin, C.; Bindi, L.; Ma, C.; Tschauner, O.; Hollister, L.S.; Steinhardt, P.J. Shock synthesis of quasicrystals with implications for their origin in asteroid collisions. *Proc. Natl. Acad. Sci. USA* **2016**, *113*, 7077–7081. [[CrossRef](#)] [[PubMed](#)]
14. Bindi, L.; Lin, C.; Ma, C.; Steinhardt, P.J. Collisions in outer space produced an icosahedral phase in the Khatyrka meteorite never observed previously in the laboratory. *Sci. Rep.* **2016**, *6*, 38117. [[CrossRef](#)]
15. Lin, C.; Hollister, L.S.; MacPherson, G.J.; Bindi, L.; Ma, C.; Andronicos, C.L.; Steinhardt, P.J. Evidence of cross-cutting and redox reaction in Khatyrka meteorite reveals metallic-Al minerals formed in outer space. *Sci. Rep.* **2017**, *7*, 1637. [[CrossRef](#)]
16. Stagno, V.; Bindi, L.; Shibazaki, Y.; Tange, Y.; Higo, Y.; Mao, H.-K.; Steinhardt, P.J.; Fei, Y.W. Icosahedral AlCuFe quasicrystal at high pressure and temperature and its implications for the stability of icosahedrite. *Sci. Rep.* **2014**, *4*, 5869. [[CrossRef](#)]
17. Stagno, V.; Bindi, L.; Park, C.; Tkachev, S.; Prakapenka, V.B.; Mao, H.-K.; Hemley, R.J.; Steinhardt, P.J.; Fei, Y.W. Quasicrystals at extreme conditions: The role of pressure in stabilizing icosahedral Al₆₃Cu₂₄Fe₁₃ at high temperature. *Am. Mineral.* **2015**, *100*, 2412–2418. [[CrossRef](#)]
18. Takagi, S.; Kyono, A.; Mitani, S.; Sugano, N.; Nakamoto, Y.; Hirao, N. X-ray diffraction study of the icosahedral AlCuFe quasicrystal at megabar pressures. *Mater. Lett.* **2015**, *161*, 13–16. [[CrossRef](#)]

19. Hong, S.T. Three-Dimensional Modeling of Quasicrystal Structures from X-ray Diffraction: An Icosahedral Al–Cu–Fe Alloy. *Inorg. Chem.* **2017**, *56*, 7354–7359. [[CrossRef](#)]
20. Parsamehr, H.; Lu, Y.J.; Lin, T.Y.; Tsai, A.P.; Lai, C.H. *In-Situ* observation of local atomic structure of Al-Cu-Fe quasicrystal formation. *Sci. Rep.* **2019**, *9*, 1245. [[CrossRef](#)]
21. Bindi, L.; Steinhardt, P.J.; Yao, N.; Lu, P.J. Natural quasicrystals. *Science* **2009**, *324*, 1306–1309. [[CrossRef](#)] [[PubMed](#)]
22. Sugiyama, K.; Hiraga, K.; Saito, K. Cubic approximants in the Al-Pd-Fe and Al-Pd-Ru systems. *Mater. Sci. Eng. A* **2000**, *294–296*, 345–347. [[CrossRef](#)]
23. Sugiyama, K.; Kato, T.; Ogawa, T.; Hiraga, K.; Saito, K. Crystal structure of a new 1/1-rational approximant for the Al-Cu-Ru icosahedral phase. *J. Alloys Compd.* **2000**, *299*, 169–174. [[CrossRef](#)]
24. Dshemuchadse, J.; Kuczera, P.; Steurer, W. A new cluster-based cubic phase in the Al-Cu-Ir system. *Intermetallics* **2013**, *32*, 337–343. [[CrossRef](#)]
25. Fujita, N. A structural reinvestigation of α -AlCuRu as merohedric twins. Presented at the Aperiodic 2018, 9th Conference on Aperiodic Crystals, Ames, IA, USA, 8–13 July 2018.
26. Simura, R.; Sugiyama, K.; Suzuki, S.; Kawamata, T. Crystal Structure of the C-AlRuNi Phase. *Mater. Trans.* **2017**, *58*, 1101–1105. [[CrossRef](#)]
27. Raghavan, V. Al-Cu-Fe (Aluminum-Copper-Iron). *JPEDAV* **2005**, *26*, 59–64. [[CrossRef](#)]
28. Raghavan, V. Al-Mn-Pd (Aluminum-Manganese-Palladium). *JPEDAV* **2009**, *30*, 71–76. [[CrossRef](#)]
29. Raghavan, V. Al-Fe-Pd (Aluminum-Iron-Palladium). *JPEDAV* **2007**, *28*, 374–376. [[CrossRef](#)]
30. Tsai, A.P.; Yamamoto, A. Quasicrystalline and crystalline phases in Al-Pd-Fe system. *Philos. Mag. Lett.* **1993**, *34*, 155–161.
31. Peterson, G.G.C.; Yannello, V.J.; Fredrickson, D.C. Inducing Complexity in Intermetallics through Electron–Hole Matching: The Structure of Fe₁₄Pd₁₇Al₆₉. *Angew. Chem. Int. Ed.* **2017**, *56*, 10145–10150. [[CrossRef](#)]
32. Edler, F.; Gramlich, V.; Steurer, W. Structure and disorder phenomena of cubic Al₃₉Fe₂Pd₂₁ in comparison with related structures. *J. Alloys Compd.* **1998**, *269*, 7–12. [[CrossRef](#)]
33. Balanetsky, S.O.; Grushko, B.; Urban, K.; Velikanova, T.Y. Physicochemical Materials Research—Ternary Cubic Phases in the Al-Pd-Fe System. *Powder Metall. Met. Ceram.* **2004**, *43*, 396–405. [[CrossRef](#)]
34. Balanetsky, S.; Grushko, B.; Velikanova, T.Y.; Urban, K. Investigation of the Al-Pd-Fe phase diagram between 50 and 100 at.% Al: Ternary phases. *J. Alloys Compd.* **2004**, *368*, 169–174. [[CrossRef](#)]
35. Balanetsky, S.; Grushko, B.; Velikanova, T.Y.; Urban, K. An investigation of the Al-Pd-Fe phase diagram between 50 and 100 at.% Al: phase equilibria at 750 °C. *J. Alloys Compd.* **2004**, *376*, 158–164. [[CrossRef](#)]
36. APEX3; SAINT; SADABS. *Software for Data Reduction, Absorption Correction and Structure Solution*; Bruker AXS Inc.: Madison, WI, USA, 2015.
37. Sheldrick, G.M. SHELXT-Integrated space-group and crystal-structure determination. *Acta Crystallogr. A* **2015**, *71*, 3–8. [[CrossRef](#)] [[PubMed](#)]
38. Sheldrick, G.M. Crystal structure refinement with SHELXL. *Acta Crystallogr. C* **2015**, *71*, 3–8. [[CrossRef](#)]
39. Akhmetshina, T.G.; Blatov, V.A. A fascinating building unit: Mackay cluster in intermetallics. *Struct. Chem.* **2017**, *28*, 133–140. [[CrossRef](#)]
40. Akhmetshina, T.G.; Blatov, V.A.; Proserpio, D.M.; Shevchenko, A.P. Topology of Intermetallic Structures: From Statistics to Rational Design. *Acc. Chem. Res.* **2018**, *51*, 21–30. [[CrossRef](#)]
41. Akhmetshina, T.G.; Blatov, V.A. Topological methods for complex intermetallics. *Z. Kristallogr.* **2017**, *232*, 497–506. [[CrossRef](#)]
42. Pankova, A.A.; Blatov, V.A.; Ilyushin, G.D.; Proserpio, D.M. γ -Brass Polyhedral Core in Intermetallics: The Nanocluster Model. *Inorg. Chem.* **2013**, *52*, 13094–13107. [[CrossRef](#)]
43. Edler, F.J. Untersuchung des ternären Systems Al-Fe-Pd auf Quasikristalle und ihre Approximanten. Ph.D. Thesis, ETH Zürich, Zürich, Switzerland, 1997.
44. Ellner, M.; Kattner, U.; Predel, B. Konstitutionelle und strukturelle untersuchungen im system PdAl. *J. Less-Common Met.* **1982**, *87*, 117–133. [[CrossRef](#)]
45. Wang, J.P.; Sun, W.; Liu, Z.Y.; Zhang, Z. Structure analysis of complex alloy phases in as-solidified microstructures of Al-Pd-Fe alloy. *Chin. J. Nonferrous Met.* **2009**, *19*, 1587–1593.
46. Kitaev, Y.E.; Panfilov, A.G.; Tasci, E.S.; Aroyo, M.I. High-symmetry phase prediction using trees of group–supergroup relations. *Phys. Solid State* **2015**, *57*, 2297–2304. [[CrossRef](#)]

47. Yaniv, G.; Fuks, D.; Meshi, L. Explanation of structural differences and similarities between the AT₂Al₁₀ phases (where A = actinide, lanthanide or rare earth element and T = transition metal). *Z. Kristallogr.* **2019**, *234*, 595–603. [[CrossRef](#)]
48. Brandenburg, K.; Putz, H. *Diamond*; Crystal Impact GbR: Bonn, Germany, 2017.
49. Grin, Y. The crystal structure of the binary iridium-aluminum IrAl_{2.75} and rhodium-aluminum RhAl_{2.63} phase. *Z. Kristallogr.* **1997**, *212*, 439–444. [[CrossRef](#)]
50. Liu, C.; Fan, C.Z. Crystal structure of the λ-Al₁₃Fe₄-type intermetallic (Al,Cu)₁₃(Fe,Cu)₄. *IUCrData* **2018**, *3*, x180363. [[CrossRef](#)]



© 2019 by the authors. Licensee MDPI, Basel, Switzerland. This article is an open access article distributed under the terms and conditions of the Creative Commons Attribution (CC BY) license (<http://creativecommons.org/licenses/by/4.0/>).